JOURNAL OF MATERIALS SCIENCE 17 (1982) 953–964

The detection of selective phase corrosion in cast nickel aluminium bronze by acoustic emission techniques

E. A. CULPAN, A. G. FOLEY*
Admiralty Marine Technology Establishment, Holton Heath, Poole, Dorset, UK

Cast nickel aluminium bronze (NAB) can suffer severe selective phase corrosion in seawater by a dealuminification process similar to dezincification in brasses. During the process, which occurs particularly in the heat-affected zones of weld repairs, copper is redeposited at the corroded areas thus making the phenomenon extremely difficult to detect by conventional non-destructive testing techniques. It was considered likely that the different fracture modes of sound material and corroded material would result in differing forms of acoustic emission during deformation. Acoustic emission monitoring was therefore carried out on tensile specimens of as-cast NAB, welded NAB and corroded NAB. The failed specimens were then examined using optical and scanning electron microscopy. It was apparent from the results that there were significant differences in the acoustic emission behaviour of the three types of material. This was revealed in characteristic event counts, event amplitudes and r.m.s. energy outputs and by normalized amplitude analysis of the data. These differences in behaviour have been correlated with the varying structures of NAB and their behaviour under stress.

1. Introduction

Cast nickel aluminium bronzes (NAB) are extensively used for marine engineering applications because of their strength, which is similar to that of medium-carbon steel, and corrosion resistance. Other valuable properties of these alloys are low magnetic permeability, low coefficient of friction resistance to softening at elevated temperatures and non-sparking nature. These alloys, of nominal composition 9.5% aluminium, 5% nickel, 5% iron and copper remainder, have replaced the binary 10% aluminium bronze alloy in many demanding applications.

The incidence of selective phase corrosion in aluminium bronze is now very well known [1–3] but nickel aluminium bronze has usually been considered to be immune from this sort of attack. However, several instances of selective phase corrosion have been observed with this material following seawater immersion [4–6], usually in the region of welds. As will be discussed later, this form of corrosion is extremely difficult to detect with conventional non-destructive testing (NDT) techniques, and accordingly some work was initiated to investigate the possibility of using acoustic emission† (AE) techniques to locate areas of selective phase attack.

It was considered likely that the acoustic emission behaviour of corroded NAB would differ from sound material due to different deformation mechanisms in the less ductile corroded areas and/or emissions from cracking in these regions. Thus, stressing a corroded component of NAB by, say, proof testing should give rise to characteristic emissions which could be used to locate the site of damage. This paper will describe aspects of this work with particular reference to the AE behaviour of corroded NAB. As NAB has

*Present address: National Institute of Agricultural Engineering, West Park, Silsoe, Bedfordshire, UK.
†Acoustic emission may be defined as a transient elastic wave generated by the rapid release of energy within the material.

0022–2461/82/040953–12$03.94/0

a complex microstructural system with which its AE and corrosion are inevitably linked, some discussion on the development of microstructure in this alloy will be included.

2. Selective phase corrosion

Selective phase corrosion is a specific form of dealloying (the process whereby one constituent of an alloy is preferentially removed leaving behind an altered residual structure). The commonly accepted mechanism for selective attack in copper-based alloys involves the dissolution of the principal alloying elements, closely followed by the redeposition or reprecipitation of one of the elements (usually copper) at favourable sites in the microstructure. Both single- and duplex-phase alloys have been observed to undergo selective attack. In single-phase alloys the corrosion attack initiates at solute-rich areas, such as the grain boundaries which are anodic to the surrounding microstructures. In duplex alloys the corrosion attack initiates in the more anodic microstructural phase, and then has the characteristics of selective phase attack. The severity of the corrosion depends on the form of the anodic phase in the structure. If it is continuous, such as a grain-boundary film, rapid penetration of the component can occur. On the other hand, if the anodic phase is discontinuous, corrosion will be restricted to the surface exposed to the environment, leaving a surface layer of the more noble phase.

The important physical difference between dealloying and other modes of corrosion is that the size and shape of the component undergoing attack is basically unchanged. The density of the redeposited metal in the corroded area is generally less than that of the original alloy, though it often occupies the same volume as the metal which was removed. Although a slight surface discolouration may accompany the corrosion attack the amount of penetration cannot often be detected other than by destructive examination, especially if the dealloying occurs as selective phase corrosion. Consequently, selective phase corrosion may be especially dangerous in highly stressed components where loss of strength occurs without detectable metal removal.

3. Microstructure of NAB

Under normal conditions binary alloys containing up to 8% aluminium solidify to form a single-phase α solid solution at room temperature, the strength and corrosion resistance being proportional to the aluminium content. Above 8 to 8.5% aluminium a second phase, β, appears in the microstructure of air-cooled castings. The dual-phase α/β alloys do not necessarily suffer a higher corrosion rate than the single-phase α-alloys and in fact generally offer a more favourable combination of strength and corrosion resistance. However, on slow cooling these alloys undergo a phase change at 565° C when the β-phase is transformed to an α and γ_2 eutectoid structure. As the γ_2 (Cu_9Al_4) phase is richer in aluminium than either the α- or β-phases it has a much lower electrode potential and corrodes rapidly in the structure. The presence of the γ_2-phase also reduces the ductility of these alloys and steps have to be taken to prevent its formation. One possibility is to heat-treat the alloy between 600 and 800° C followed by a rapid air-cool or quench, which suppresses the β transformation, but unless the cooling rate is sufficiently rapid the γ_2-phase may still be formed. Another method is to add alloying elements that retard the formation of γ_2 while maintaining the high strength properties that characterize aluminium bronze. The principal alloying elements used for this purpose are nickel and iron. Both these elements combine with aluminium to form a complex phase, designated kappa, κ, which effectively increases the amount of aluminium that can be present in an alloy before the γ_2 phase is encountered, as shown in Fig. 1 (from the work of Cook *et al.* [7]).

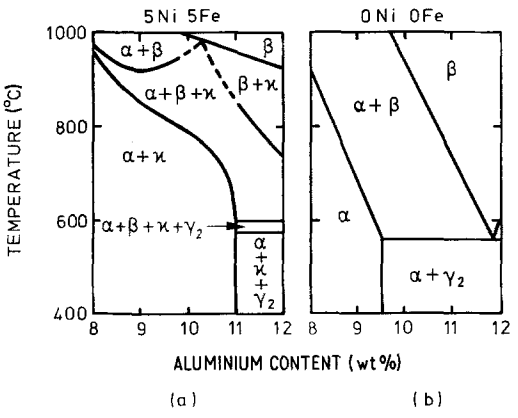

Figure 1 (a) A vertical section through the Cu–Al–Ni–Fe quaternary system at 5% Ni, 5% Fe. (b) A portion of the binary Cu–Al system.

Fig. 2 shows an optical micrograph of a typical as-cast NAB structure. It consists of light-coloured α grains and the κ-phase, present in a variety of

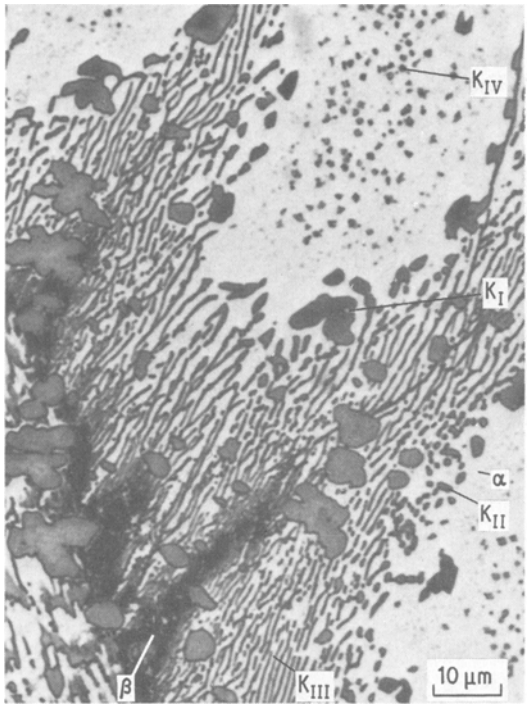

Figure 2 A typical as-cast microstructure of nickel aluminium bronze showing the constituent phases.

morphological forms. The large, grey-coloured globular or rosette particles, designated κ_I, are iron-rich and based on the Fe_3Al structure. The proeutectoid structure of lamellar κ_{III} and globular κ_{II} and α is formed by decomposition of the remaining β between the α grains. On further cooling a fine precipitation of κ_{IV}-phase is produced within the α grains. κ_{IV} is also iron-rich, based on Fe_3Al, and κ_{III} and κ_{II} are based on NiAl–FeAl. Frequently there is a small amount of retained β present within the proeutectoid structure.

Recent work [4–6] has shown that whilst NAB does not suffer from any of the problems associated with γ_2 formation, it can suffer a form of selective phase corrosion. This corrosion occurs at the eutectoid structure, leaving a porous copper phase occupying some of the vacant areas, as shown in Fig. 3. As the eutectoid is continuous throughout the material, significant corrosion penetration can take place without causing obvious surface degradation. This attack is particualrly pronounced in the band of parent metal just outside the heat-affected zones of welds. It can be seen that much of the proeutectoid α and κ_{II} and κ_{III} phase has been removed and copper has been redeposited

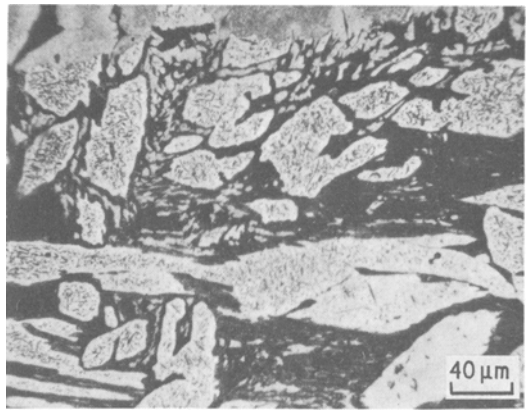

Figure 3 Selective phase attack of nickel aluminium bronze following seawater immersion, showing areas of redeposited copper.

to occupy the vacant areas. As the proeutectoid phase is continuous throughout the material, significant corrosion penetration can take place without causing any pronounced surface degradation. It has been shown using scanning electron microscopy [6] that it is the α-phase, which is anodic to the adjacent κ_{III} lamellae, which is preferentially attacked. This leads to the eventual removal of the peoeutectoid phase. This attack is particularly pronounced in the band of parent metal just outside the heat-affected zones of welds. It is suggested that this is due to presence of residual welding stresses which accelerate the anodic dissolution by opening up the corroded areas to allow continued ingress of corrodant or by disrupting the protective oxide film that generally protects NAB.

4. Experimental materials and methods

4.1. Materials

The investigation was carried out using flat plates of NAB of approximate dimensions 400 mm × 200 mm × 12 mm. The plates were sectioned into two halves in the longitudinal direction and the pieces butt welded with a vertical preparation, using the metal–inert gas (MIG) process and matching filler wire. Chemical analysis of the cast and weld metal used are shown in Table I; both weld metal and casting conform to BS1400 AB2.

Tensile test pieces were machined from the cast plates and from the welded plates, and had an elongated head to accomodate the AE transducer. The welded specimens were cut so that the weld

TABLE I Chemical analysis of cast NAB and weld metal

Condition	Al	Fe	Ni	Mn	Si	Pb	Sn	Cu
Casting	9.16	4.98	4.95	1.34	< 0.01	< 0.01	< 0.01	Remainder
Weld	8.75	4.25	4.66	1.06	< 0.01	< 0.01	< 0.01	Remainder

was across the middle of the gauge length. The tensile test pieces were clamped in a NAB frame and immersed in the seawater of Portland Harbour. Control specimens were used to follow the rate of attack and some of the tensile specimens were removed when the corrosion had affected approximately 25% of the cross-sectional area. Other specimens have been left in the sea for enhanced attack to take place. Tensile tests were carried out on five specimens in both the as-cast and corroded conditions, and on two as-welded specimens.

4.2. Mechanical testing

Tensile tests were performed on a 200 kN capacity Zwick Universal Testing Machine, model 1484, using a constant cross-head displacement rate of 0.5 mm min^{-1}. Load against elongation was plotted automatically on a Hewlett Packard X–Y chart recorder, model 704A, linked to the testing machine.

4.3. AE Instrumentation

The acoustic emission instrumentation used in the tests is shown schematically in Fig. 4. A piezoelectric transducer, with a resonant frequency of 400 kHz, was used in all the tests. Signals from the transducer were amplified by a preamplifier and a main logarithmic amplifier with a total gain of 97 dB (at 400 kHz). The signal threshold level was set at 1.3 V, giving a minimum detectable signal level of 18 μV at the transducer. An event count was recorded when the peak amplitude of an emission exceeded the signal threshold level during the sampling time of the system (~ 1.6 msec).

The system is capable of monitoring AE event and ring-down count data and signal amplitude distributions, all of which are fed, together with mechanical test data, e.g. applied load, into a Hewlett Packard 2100S minicomputer. The r. m. s. signal level, though not recorded by the computer, was also monitored during the tests by passing the signal from the main amplifier through an r. m. s. converter and plotting the resulting signal on a chart recorder. On-line plots of, for example, number of AE events against time and load against time can be displayed during the test on a visual display unit (VDU). The amplitudes of captured signals are transferred from the main amplifier to the computer where they are digitized and held in the memory. Consequently, cumulative amplitude distributions can be stored at any time during the test by dumping the information stored in the

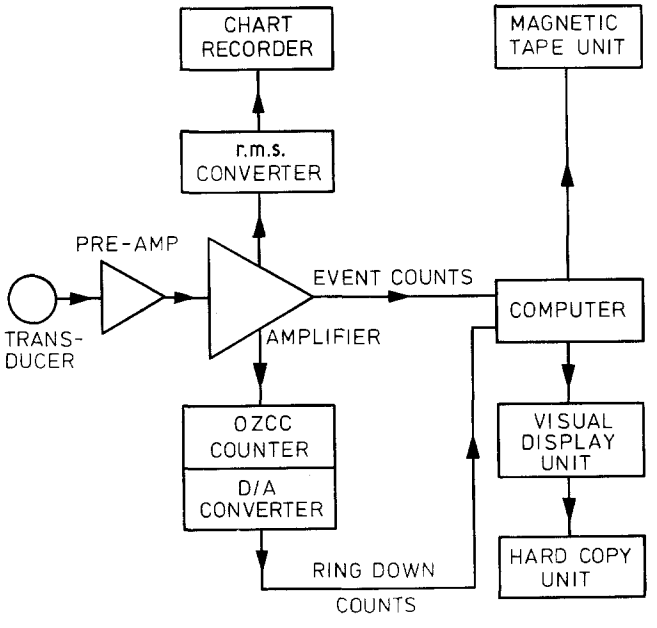

Figure 4 Schematic illustration of the acoustic emission monitoring equipment.

TABLE II The ranges of mechanical properties for nickel alumium bronze in the conditions studied

Condition	0.2% proof stress ($MN\,m^{-2}$)	Ultimate tensile stress ($MN\,m^{-2}$)	Engineering fracture strain
As-cast	197–227	548–559	0.174–0.208
Welded	288–301	582–583	0.107–0.115
Corroded	257–278	373–466	0.020–0.048

computer memory on to paper tape. The final amplitude distribution for the whole test is also stored on magnetic tape together with the other AE and mechanical test data.

Since only two parameters can be monitored on-line during the test, the storage of the data either on magnetic or paper tape permits post-test plots of the other recorded data to be displayed on the VDU from which permanent hard copies can be made. Both discrete and cumulative amplitude distributions for a particular period of the test can be redrawn, when the digitized values of amplitude can be converted to a decibel range. The maximum number of AE events that could be recorded during the tests was 600 per second. This is controlled by the time required for peak signal detection, digitization and storage, and system reset, i.e. to allow the captured signal to decay below the threshold level before accepting another AE event. Prior to each test, use was made of the helium gas jet apparatus [8, 9] to ensure reproducibility of transducer–specimen coupling. The specimen was excited by the gas jet under standard pressure and the amplitude detected by the amplifier recorded.

5. Results

The range of mechanical properties for the three conditions studied are shown in Table II. These are consistent with those expected in NAB, with the fine-grained, higher-strength welded region giving some additional strength. The relatively low ultimate tensile stress (UTS) and elongation of the corroded specimen indicates clearly the influence of the selective phase attack and the redeposition of copper, of little strength, at the grain-boundary regions.

Examination of the broken ends of the test pieces using scanning electron and optical microscopy revealed certain characteristic features of fracture. The uncorroded specimens, whether welded or not, always failed in the as-cast parent plate. The weld region was relatively undeformed, though extensive deformation took place in the adjacent parent plate. As expected, the fracture surfaces of both specimens were similar in appearance, showing the normal ductile failure mode characteristic of NAB. Final fracture in as-cast NAB frequently occurred by shearing across a plane of large κ_I particles, as shown in Fig. 5. Small surface cracks were evident away from the fracture surface at 45° to the surface of the test piece, the direction of maximum resolved shear stress, and not following the line of the lamella κ_{III} phase.

The fracture behaviour of the corroded specimens was completely different to the other specimens. Failure always occurred at the weld–parent metal interface just outside the heat-affected zone. Optical microscopy has shown the significant influence of selective phase attack on the deformation mechanism. At the fracture edge (Fig. 6) it is obvious that crack propagation has followed the grain-boundary proeutectoid phase where redeposition of copper has taken place. Away from the facture surface there is also evidence of cracking through the copper caused by the stress applied during the test. The fracture surfaces of the corroded specimens showed two distinct areas.

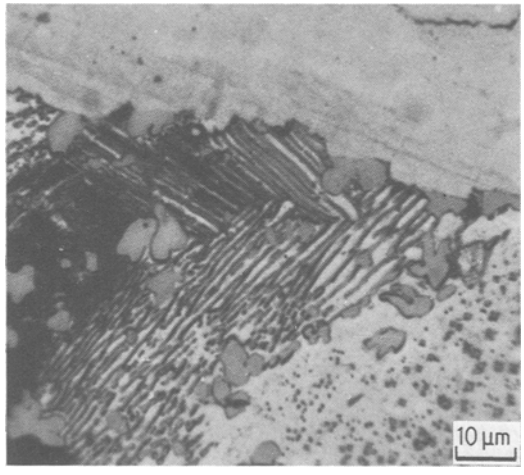

Figure 5 Fracture of an as-cast specimen showing the shearing of κ_I particles.

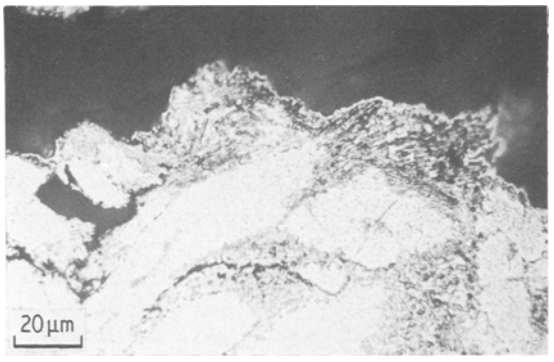

Figure 6 Fracture of a corroded specimen showing presence of redeposited copper on fracture surface.

The area where there had been no corrosion attack showed normal ductile failure whereas the area of corrosion showed the influence of the relatively brittle phase at the α grain boundaries, as in Fig. 7a. Closer examination of this surface, as in Fig. 7b, showed that the redeposited copper is a honeycomb structure through which a crack can rapidly propagate. This also explains why the redeposited copper is able to occupy the volume of alloy removed by corrosion, thus making detection of this attack extremely difficult.

6. AE results

The acoustic emission data was displayed on-line in the form of graphs of AE events sec^{-1} with time and applied load with time. Typical on-line plots for the three conditions investigated are shown in Fig. 8a to c. It can be seen that there were significant differences between the specimens, particularly in terms of the test times and number of AE events. The influence of the corrosion attack was to significantly reduce the ductility of the test piece giving a relatively short time of test. The welded specimen test was influenced by the area of higher-strength weld metal within the gauge length, which reduced the elongation and hence the time of test compared with the as-cast specimens.

There was a significantly greater number of AE events in the as-cast specimen with a peak just prior to the 0.2% proof stress of the specimen. The welded specimen showed a smaller peak, again just prior to the 0.2% proof stress, which has been associated with the volume effect of the relatively undeformed welded area in the test piece. The corroded specimens showed the least number of cumulative events up to yield, although, as will be seen later, a significant number of these events were of high amplitude.

Typical r. m. s. voltage outputs as the test progressed are shown in Fig. 9a to c for the three conditions investigated. They clearly illustrate the AE behaviour of the specimens through the different stages of the tensile test. The as-cast specimen showed a high r. m. s. voltage peak (~450 mV) just prior to the 0.2% proof stress. This relatively smooth curve had the characteristics of continuous emission, i.e. a general shift in r. m. s. level with no superimposed spikes. The r. m. s. signal level then fell from its peak value and remained comparatively steady for much of the test until shortly before failure when burst emissions were generated which appeared as spikes on the r. m. s. trace. The uncorroded welded specimens showed a similar trend except that the magnitude of its peak just prior to the 0.2% proof stress was very much reduced (~200 mV). This

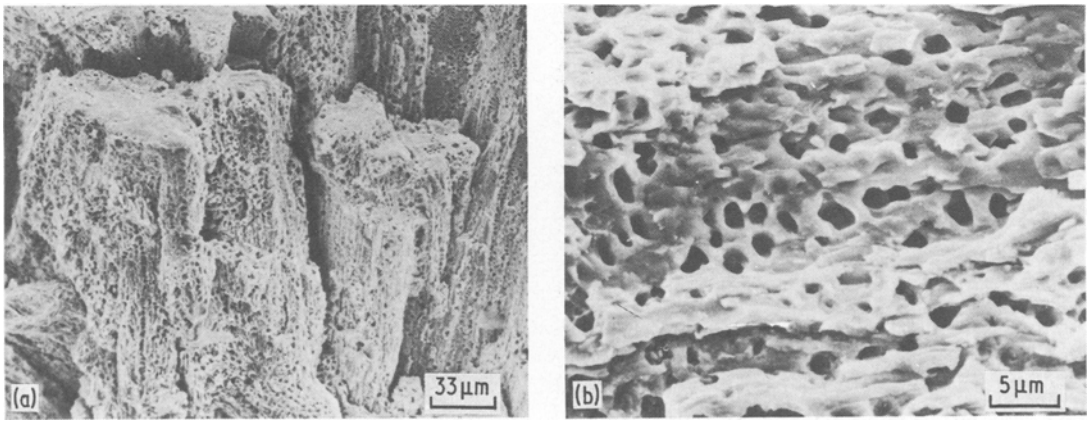

Figure 7 Fracture appearance of redeposited copper (a) general view, (b) enlargement.

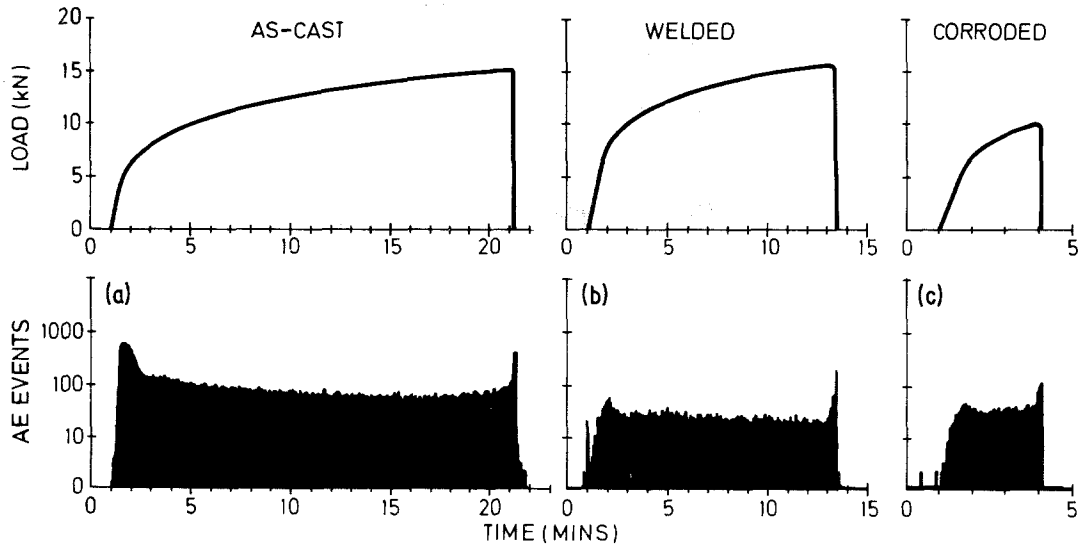

Figure 8 Typical on-line plots of acoustic emission events plotted against time and load plotted against time for: (a) as-cast condition, (b) as-welded condition, (c) welded and corroded condition.

is attributed to the volume of yielded material being much less with this condition. The corroded specimen also showed a reduced peak (~ 185 mV) prior to the 0.2% proof stress for the same reason. However, also evident are a considerable number of burst emissions throughout this test. This indicates the presence of more acoustically active deformation processes throughout the test, and not just prior to failure as in the case of the as-cast specimens and welded specimens.

Evidence that the corroded specimen condition produced a greater proportion of high-amplitude emissions compared to the as-welded condition is given in Fig. 10, which shows the number of AE events plotted against amplitude in a histogram format, for stresses up to the peak in the r. m. s. signal level. Another means of characterizing amplitude distribution which has its origin in seismology has been proposed [10], since experimental AE amplitude data often approximate to a power-law distribution of the form

$$n(a) = \left(\frac{a}{a_0}\right)^{-b}, \qquad (1)$$

where $n(a)$ is a function which can be defined as the fraction of the emission population whose peak amplitude exceeds the value a. a_0 is the lowest detectable amplitude and b is the exponent which characterizes the amplitude distribution. In fact, b is the slope of the plot of $\log n(a)$ against $\log (a/a_0)$, and has a simple physical basis. If deformation proceeds by a small number of large steps with little intervening activity, there is a larger proportion of high-amplitude emissions and a small b-value results. However, when deformation proceeds in a large number of small steps, there are more smaller amplitude emissions, and a large b-value is found. Typical examples of the above type of amplitude analysis are shown in Figs 11 and 12, for the portion of the test up to the peak in the r. m. s. signal level and for the whole test, respectively. It can clearly be seen that different b-values occur throughout the period of the test for the three specimen conditions, and that these differences can be used to distinguish those conditions.

Pseudo-AE energy values have also been determined for each test condition, by calculating the change in r. m. s. signal level from the base level at start of test and squaring this value. These values have been plotted against the applied stress for each test condition up to a stress level of 340 MN m^{-2} and are shown in Fig. 13. It can clearly be seen that the maximum in AE energy for each condition occurred at markedly different levels of applied stress and, in each case, prior to the 0.2% proof stress.

7. Discussion

The AE event rate data obtained on-line did not reveal any significant difference between the welded and uncorroded, and the welded and corroded conditions. The as-cast condition was

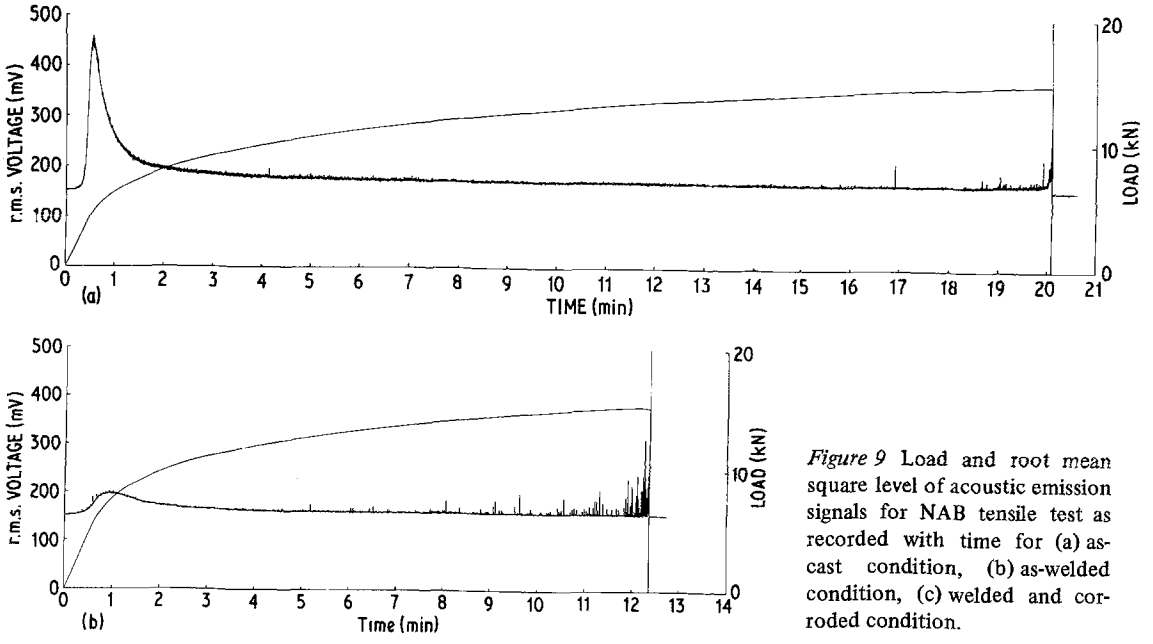

Figure 9 Load and root mean square level of acoustic emission signals for NAB tensile test as recorded with time for (a) as-cast condition, (b) as-welded condition, (c) welded and corroded condition.

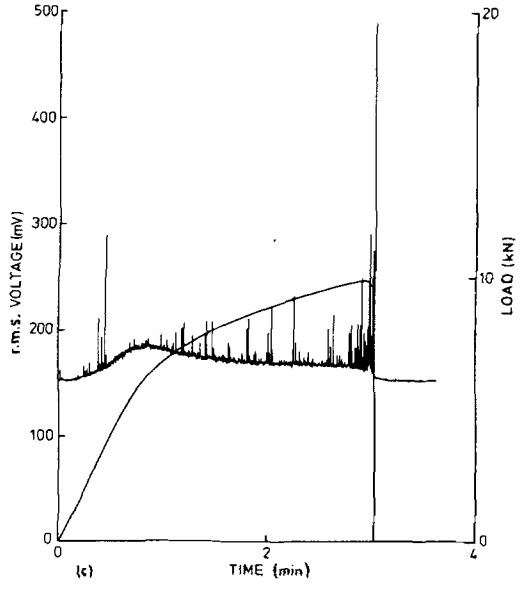

markedly different in that it gave almost an order of magnitude increase in the number of events detected as the specimen yielded. However, it seems likely that this difference arose purely from a volumetric effect since the gauge length of the two welded conditions contained a considerable proportion of weld metal (approximately 40%), and the majority of the deformation, and indeed the final failure, occurred within the parent as-cast metal for each of the three conditions tested.

In view of the application of AE techniques to proof testing on real structures, the main emphasis in the analysis of the test data obtained has centred on the portion of the tensile test up to and around the 0.2% proof stress. For this reason, a detailed study of the r. m. s. signal level and the event amplitude distributions up to the 0.2% proof stress level for each of the three test conditions was undertaken.

A simple histogram of AE events against amplitude taken at approximately the 0.2% proof stress level reveals the differences between the three conditions tested as seen in Fig. 10. The greater numbers of higher-amplitude emissions in the corroded situation compared to the as-welded case can be observed. However, the suitability of using a normalized amplitude distribution approach is highlighted here, since the as-cast condition gave rise to an order of mangitude more events over the whole amplitude range than either of the other two conditions which were almost identical, and hence can influence a qualitative interpretation.

In this latter approach, the numbers of events whose peak amplitude exceeds a given value are normalized by the total number of events included in the histogram. This ensures that the differences in the total numbers of AE events, both up to the proof stress level and over the whole test, for the three conditions are taken into account. In both the part-test and whole-test plots of the welded and corroded specimens, the best-fit straight lines had correlation coefficients better than −0.990, though this dropped to −0.970 for the

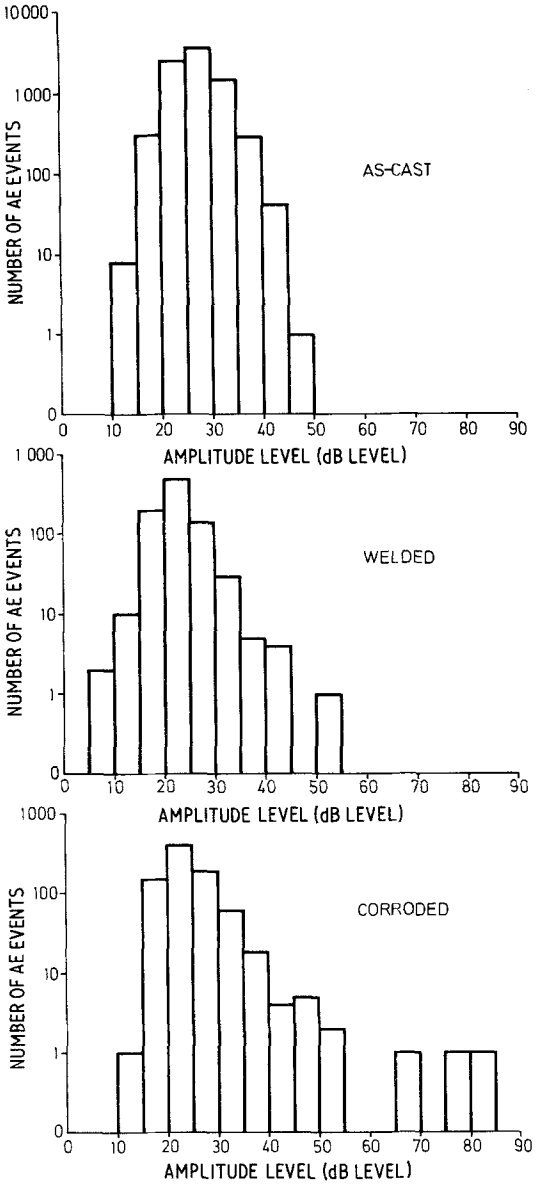

Figure 10 Typical amplitude histograms for each condition studied, up to the peak in the r. m. s. signal level.

as-cast condition. The distinction between the b-values for all three conditions is quite evident at both intervals of the test and indicates that there is a decrease in the level of high-amplitude AE in the order: corroded, welded, as-cast. This trend was confirmed in further tests of the three conditions, though the nature of the cast material and, where appropriate, the extent of corrosion attack, did produce specimen-to-specimen variations in the measured b-value for each condition.

The b-value for the as-cast specimen showed a decrease as the tensile test progressed; in fact, the data for the whole test case was best described by two distinct power-law relationships, see Fig. 12. The best-fit line at the high-amplitude end of the spectrum for the whole test data had the lowest b-values of all at 0.47, indicating a large proportion of high-amplitude events over the range 50 to 100 dB. Thse high-amplitude events were completely absent up to the 0.2% proof stress, as in Fig. 11, a fact which is also revealed on the r. m. s. trace for this test (Fig. 9a), which only had significant spikes superimposed on the general signal level very close to the final fracture. These high-amplitude events just prior to failure are associated with the fracture of the globular κ_I particles, as in Fig. 5. The large b-values in both the part-test data and the low-amplitude end of the whole-test data for the as-cast condition reflect the predominance of low-amplitude, continuous-type emission, most prevalent at and around yield, but also present throughout the majority of the test. These low-amplitude emissions are attributed to plastic deformation within the α matrix.

The b-values for the welded, and welded and corroded specimens are significantly different both up to the 0.2% proof stress and over the whole test, though the values tend to converge as the test proceeds, see Figs 11 and 12. This is probably due to the increase in the frequency of higher-amplitude, burst-type emissions in the welded specimen with increasing strain, as shown in the r. m. s. trace (Fig. 9b).

The specimens containing a weld, i.e. both uncorroded and corroded cases, have restricted plastic deformation and both eventually fracture within parent metal. As such, the uncorroded weld specimen could be considered as a special case of the as-cast specimen. However, the effect of the less ductile weld metal would appear not only to restrict plastic deformation to the neighbouring parent material, but also to give rise to a greater proportion of high-amplitude emissions, as evidenced by the lower b-values, the difference being greater as the applied strain increases (compare Figs 11 and 12). It has been tentatively suggested that these higher-amplitude emissions arise from deformation within the weld heat-affected zone once the work-hardening capacity of the as-cast ligaments has been exceeded.

The presence of selective phase corrosion within the welded material is indicated by the smaller b-values evident during the whole test,

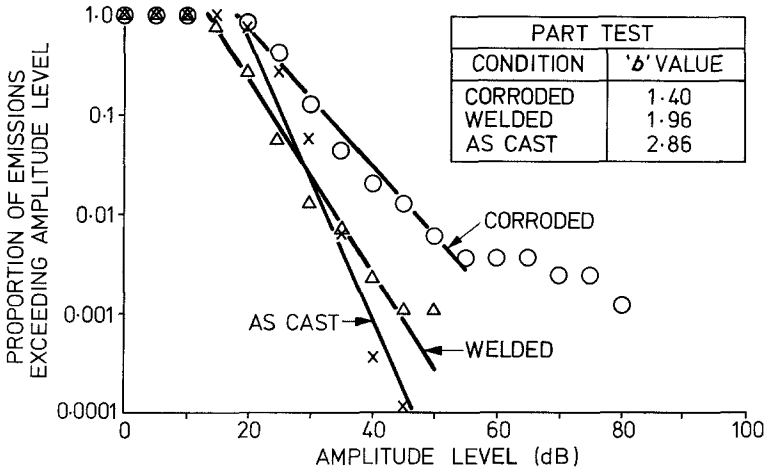

Figure 11 Typical normalized amplitude histograms for the three conditions studied, up to the peak in the r.m.s. trace.

confirming that a greater proportion of the events which occur are of higher amplitude than in the uncorroded situation. The corroded specimens rapidly undergo cracking in the corroded areas due to the presence of the less ductile copper phase which is redeposited during the corrosion reaction. Visible cracking is evident on the surface of the specimen very early on in the tensile test, and it seems reasonable to associate the higher-amplitude, burst-type emissions with rapid crack propagation through the redeposited copper areas, which have little resistance to cracking.

The data for AE energy against applied stress also revealed significant differences between the three material conditions under consideration (see Fig. 13). This analysis ignored any burst-type emissions which occurred, simply concentrating on the mean r. m. s. signal level for calculations. Consequently, deformation processes occuring by smaller numbers of discrete steps would be indicated by smaller values of AE energy, whilst those occurring by larger numbers of more continuous steps would yield large values of AE energy. Thus, this type of energy analysis supports the model proposed using the amplitude power-law relationship that the corroded specimen emits a greater proportion of higher-amplitude emissions, and hence less AE energy (as defined earlier), as it yields than does the welded specimen. It is interesting to note that the peak in the AE energy occurred at different levels of applied stress; this again is probably due to the restraining effect of the weld metal when comparing the as-cast condition to either of the welded conditions. Also, since the redeposited copper in the corroded areas has little strength, the load-bearing capacity of the

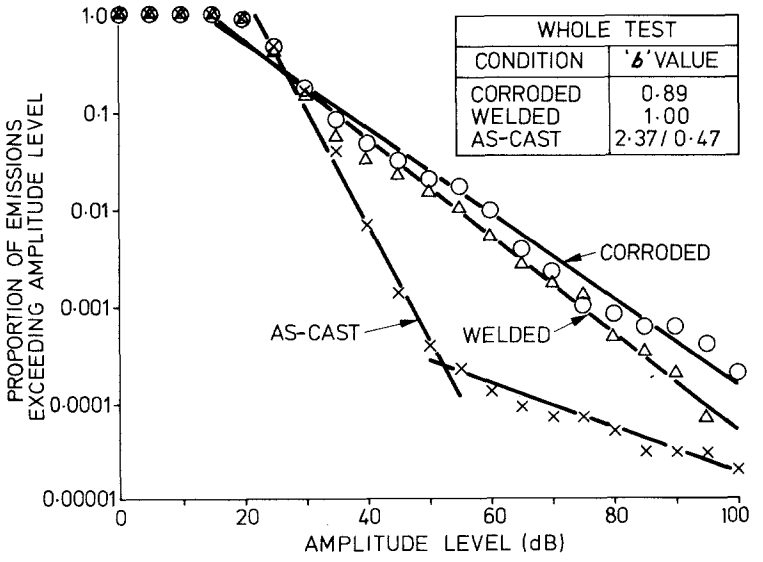

Figure 12 Typical normalized amplitude histograms for the three conditions studied, taken over the whole test.

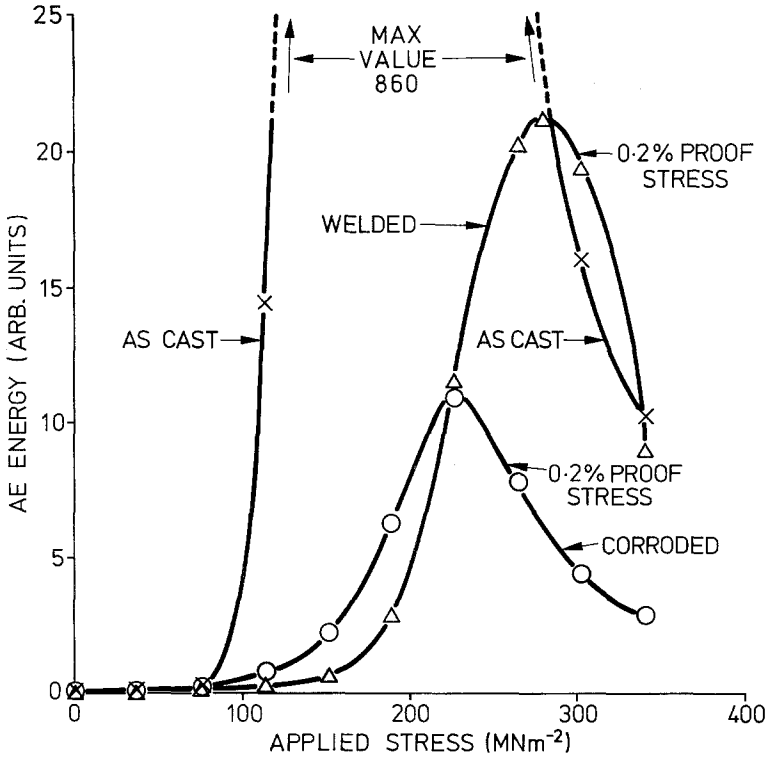

Figure 13 Acoustic emission energy plotted against applied stress for each condition studied.

corroded specimen will be reduced, thereby lowering the apparent applied stress, and causing a shift in the maxima of the energy curves for the two welded conditions.

8. Conclusions

(a) Tests on tensile specimens have shown the potential of acoustic emission techniques to detect the presence of selective phase attack in nickel aluminium bronze.

(b) It has been shown that normalized amplitude distribution plots can be characterized using a single parameter, b, which is the slope of the distribution plot.

(c) Clearly distinguishable values of the parameter b were found for the three test conditions studied, bot up to the 0.2% proof stress level and for the whole test, including the final failure.

(d) The differences between the b-values for the three test conditions indicated that there was a decrease in the proportion of high-amplitude acoustic emissions in the order: welded and corroded, as-welded, as-cast.

(e) The greater proportion of high-amplitude emissions in the case of corroded specimens has been attributed to rapid crack propagation through the less ductile, redeposited copper phase.

(f) Acoustic emission energy analysis also supports the evidence from the normalized amplitude distribution plots that corroded specimens emit a greater proportion of higher-amplitude, burst-type emissions during the elastic loading and yield region than either of the other two conditions investigated.

Acknowledgements

The authors wish to thank Mr M. Last and Mr M. Brewer for their assistance during this investigation. Any views expressed are those of the authors and do not necessarily represent those of the Procurement Executive, Ministry of Defence.

References

1. B. UPTON, *Corrosion* 19 (1963) 204t.
2. J. C. ROWLANDS, *Corrosion Sci.* 2 (1972) 87.
3. P. J. MACHEN and A. A. SMITH, *CDA Publication 31* (1966) p. 111.
4. G. NEWCOMBE, C. DIMBYLOW and R. JONES, Proceedings of the Conference on Welding of Castings, Bradford, 1976 (Welding Institute, Cambridge, 1977) p. 199.
5. C. A. ZANIS and R. J. FERRARA, *Trans. Amer. Foundryman Soc.* 82 (1974) 74.
6. E. A. CULPAN and G. ROSE, *Brit. Corros. J.* 14 (1979) 160.

7. M. COOK, W. P. FENTIMAN and E. J. DAVIES, *Inst. Metals* 80 (1951–52) 419.
8. S. L. McBRIDE and T. S. HUTCHINSON, *Can. J. Phys.* 54 (1976) 1824.
9. M. N. BENTLEY and G. GREEN, Paper presented at the Institute of Acoustics Conference, Chelsea College, London, 1976.
10. A. A. POLLOCK, *Non-Destructive Testing* 6 (1973) 264.

Received 20 May
and accepted 18 August 1981